EVOLUTION OF FINITE VORTICITY STRIPS USING A NON-DIVERGENT, BAROTROPIC MODEL

Matthew T. Vaughan* and Thomas A. Guinn
Embry-Riddle Aeronautical University, Daytona Beach, FL

1. INTRODUCTION

There have been several studies that examine the breakdown of the Inter-Tropical Convergence Zone (ITCZ). The dry dynamics of ITCZ breakdown has been examined using shallow-water equations (SWE) on an *f*-plane (Guinn and Schubert, 1993), using the SWE on a sphere (Ferreira and Schubert, 1997), and using a primitive equation model (Wang and Magnusdottir, 2005). Wang et al. (2010) examined the process in a moist atmosphere.

This study seeks to enhance the understanding of how various finite vorticity strips evolve using a non-divergent, barotropic, pseudo-spectral model on both an *f*-plane and β-plane. The model allows the initial vorticity field to be specified in a variety of geometric shapes without use of a forcing function. A variation of this model was developed in FORTRAN by Schubert et al. (1999). This paper examines the evolution of finite length vorticity strips and explores the effect of length, width, and the length-width ratio of the strips on vortex development. In addition, vortex development is compared using an *f*-plane and a β-plane.

2. MODEL DETAILS

The non-divergent, barotropic model is governed by the following momentum and mass-continuity equations:

$$\frac{\partial u}{\partial t} + u\frac{\partial u}{\partial x} + v\frac{\partial u}{\partial y} - fv + \frac{1}{\rho}\frac{\partial p}{\partial x} = \nu\nabla^2 u, \quad (1.1)$$

$$\frac{\partial v}{\partial t} + u\frac{\partial v}{\partial x} + v\frac{\partial v}{\partial y} + fu + \frac{1}{\rho}\frac{\partial p}{\partial y} = \nu\nabla^2 v, \quad (1.2)$$

$$\frac{\partial u}{\partial x} + \frac{\partial v}{\partial y} = 0, \quad (1.3)$$

where u and v are the zonal and meridional components of the wind, p is the pressure, and ρ is the constant density. The non-divergent, mass-continuity equation allows the u and v-wind components to be expressed in terms of the stream function: $u = -\partial\psi/\partial y$ and $v = \partial\psi/\partial x$. The above equations can be reduced to a single predictive equation in ψ. The vorticity equation can then be expressed as

$$\frac{\partial \zeta}{\partial t} + \frac{\partial(\psi,\zeta)}{\partial(x,y)} = \nu\nabla^2\zeta, \quad (2)$$

where $\zeta=\nabla^2\psi$ is relative vorticity and $\partial(\cdot,\cdot)/\partial(x,y)$ is the Jacobian operator. The term $\nabla^2\psi$ is easily inverted using spectral methods to obtain ψ. In the absence of diffusion, vorticity is materially conserved, analogous to PV conservation in the shallow water framework. The variable ν is the coefficient of diffusion. Ordinary diffusion is used to prevent spectral blocking. When the β-plane approximation is used, the term $-\beta(\partial\psi/\partial x)$ is added as a forcing term to the right-hand side of (2).

Equation 2 is solved on a doubly periodic square grid with 512 collocation points (*N*) spread across 6400 km (*L*) in both the *x* and the *y* directions. To prevent aliasing of quadratically non-linear terms, the maximum wave number, w_{max} was chosen according to

$$w_{max} = \frac{N-1}{3}. \quad (4)$$

Using 512 grid points, w_{max} is 170, which yields an effective resolution of approximately 37 km. The diffusion coefficient ν is determined such that waves with total wave number w_{max} e-fold in one-hour. For all simulations, this equates to 9,972 m^2/s.

MatLab is chosen for its matrix manipulation ability and relative ease to learn. The model is broken into four parts: 1) an initialization routine that builds the vorticity arrays, 2) a time integration routine, 3) a function to calculate the derivatives in spectral space, and 4) a plotting routine.

The initialization routine builds a two dimensional vorticity array with the number of grid points in each direction, *N*, and the total domain length in meters, *L*, specified by the user. The initialization routine also creates an initial vorticity field in the center of the model domain. The finite vorticity strips are characterized by a defining half-length in meters, *x1,* a half-length indicating at what distance, *r1*, vorticity begins to decrease from its maximum value, ζ_0, a distance over which vorticity transitions from ζ_0 to zero, *r2*, and an aspect ratio, *a*, to control the ellipticity of the strip ends.

*Corresponding author address: Matthew T. Vaughan, Embry-Riddle Aeronautical Univ., Department of Applied Aviation Sciences, 600 S. Clyde Morris Blvd, Daytona Beach, FL 32114. Email: vaugham1@erau.edu

From these parameters, the finite vorticity strips are created using the below shape function r.

$$r = \begin{cases} \sqrt{a^2(|xt| - x1)^2 + (yt)^2} & \text{for } |xt| > x1 \\ |yt| & \text{otherwise,} \end{cases}$$

where $xt = x - x_0$, $yt = y - y_0$, and (x_0, y_0) defines the center of the domain.

Using the above shape function, the initial vorticity field is specified as:

$$\zeta = \begin{cases} \zeta_0 & \text{if } r \le r1 \\ \zeta_0 H(r) & \text{if } r2 > r > r1 \\ 0 & \text{if } r \ge r2 \end{cases}$$

where $H(r) = 1 - 3w^2 + 2w^3$,

and $w \equiv \frac{r - r1}{r2 - r1}$,

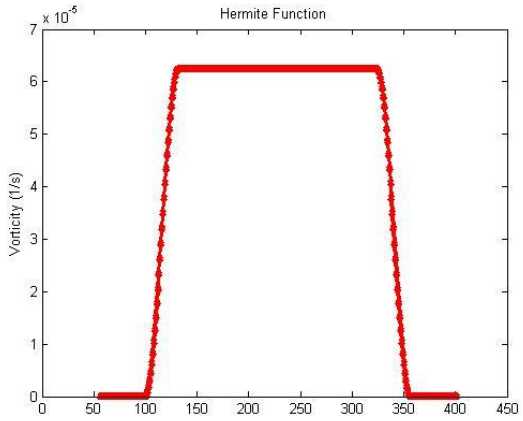

Figure 1.) Hermite function used for the initialization file. The initial vorticity, ζ_0, is set to 6.25×10^{-5} s^{-1}, *r1* is set to 150km and *r2* is set to 200km.

The function, *H(r)*, is a Hermite shape function that has the advantage of having a zero slope at r_1 *and* r_2 and smoothly transitions from one to zero going from *r1* to *r2*. The function is applied to the entire perimeter of the vorticity strip, giving a uniform transition from ζ_0 to zero (Fig. 1). The resulting vorticity field develops a "Twinkie"-shaped vorticity field. The routine outputs a .mat file containing the initialization parameters listed above and the vorticity array for use by the main model routine. Note that in order for the net circulation in the domain to equal zero, as required by the periodic boundary conditions, the area average vorticity of the initial vorticity field must be zero. Thus small negative vorticity values exist outside the vorticity strip, causing a small amount of adverse shear.

The time integration routine specifies model run-time parameters including time-step length, *dt*, number of time-steps, *tmax*, and output time intervals, *tsave*. When the β-plane option is used, β is calculated at a latitude of 10°.

Time differencing is done using a third-order Adams-Bashforth (AB3) scheme. A fourth-order Runge-Kutta (RK4) scheme was implemented initially, but upon comparing the two schemes, the AB3 was found to be significantly faster while maintaining similar solutions to the RK4. Prior to the time-integration, the array of vorticity values, *zeta*, is passed to another routine that calculates the forcing terms, i.e. diffusion and the Jacobian operator.

The spatial derivatives of vorticity and the stream function must be computed each time-step. To do this, a standard, two-dimensional, fast Fourier transform is applied to the given vorticity array, converting the vorticity field into spectral coefficients. Wave numbers greater than w_{max} are zeroed out to minimize aliasing. Calculations for the derivatives of ψ and ζ are reduced to simple multiplication. After the derivatives are calculated, they are transformed back into physical space using an inverse fast-Fourier transform. The forcing term is calculated with or without β depending on the user's specifications. The result is passed back to the main routine for time integration in physical space. Output is collected in an array at user-specified intervals and saved in a .mat file for display.

3. RESULTS

Several experiments were examined in this study. The first experiment was designed to determine the nature of "Twinkie"-shaped finite vorticity strip breakdown under constant ζ_0 on an *f*-plane. Various widths, ranging from 100 km to 400 km were tested over time period of 10 days. The domain period, ζ_0, *r2*, and *a* were held constant at 6400 km, 6.25×10^{-5} s^{-1}, 50km, and 1.0, respectively for each simulation run.

At the beginning of the simulation, the strips began rotating in a cyclonic fashion (Fig. 2a). Two notable centers of high vorticity form and rotate around a central point (Fig. 2b). At this point, the finite vorticity strips evolved into one of three forms. Strips either roll up into one circular vortex (Fig. 3a), separate into two independent vortices (Fig. 3b), or are in the process of merging into one vortex (Fig. 3c). With the given model domain length and vorticity strength, breakdown into 3 or more vortices was not observed in the *f*-plane experiments. Smaller widths tended towards rolling up

into one vortex by the end of the simulation period. Table 1 illustrates this by the high length to width ratios needed to cause vortex separation. However, as width increases, the critical ratio for vortex separation lowers. Therefore, wider strips tend to separate into two vortices more readily, requiring a smaller length to width ratio than a similarly proportioned, thinner strip (Table 1). There is no linear correlation between length-to-width ratios and vortex evolution across different widths.

Vorticity Evolution Ratios				
Width (km)	One	Merging	Separate Centers	Independent Vortices
100	1–12	12–14	14–20	20+
150	1–9	9–11	11–14	14+
200	1–8	8–9	9–13	13+
250	1–6	6–7	7–11	11+
300	1–6	6–7	7–10	10+
400	1–6	6–7	7–9	9+

Table 1. The given values indicate whether an initial vorticity strip of a certain ratio and width will roll up into one vortex, be in the process of merging into one vortex, form a conjoined area of high vorticity with two separate centers, completely separate into two vortices after 10 days

The width of the vorticity strips has a notable effect on the size of the vortices. Thinner strips tended to form weaker vortices than thicker strips (Figs. 4a and 4b). Strip length has an equally noticeable effect on the size of the vortices that develop after vortex separation. Longer strips tended to form broader areas of vorticity than shorter strips of equal width (Figs. 5a and 5b).

In the cases examined above, wider strips resulted in larger maximum winds. A second set of experiments were conducted which adjusted ζ_0 to maintain constant maximum winds. The user inputs a maximum initial wind and the model derives the maximum value of vorticity, ζ_0 using the wind and the width of the vorticity "Twinkie". For strips of equal dimensions, constant wind experiments yielded the same pattern of vortex evolution results as the constant vorticity experiments, but evolved at a different speed. If ζ_0 was higher than 6.25×10^{-5} s^{-1} used in the constant vorticity experiments, the vortex separation or roll up occurred more quickly in the constant maximum wind case. Likewise, constant wind cases with vorticity lower than 6.25×10^{-5} s^{-1} developed more slowly and did not evolve to the same extent due to the 10-day time constraint. In addition, no differences in vortex size were observed.

When β is added to the experiments, the results diverge significantly from the previous two experiments. A latitude of 10°N is used to calculate β. Once the simulation begins, vorticity immediately begins to pool towards the ends of the strip with a tendency towards the west side of the domain (Fig. 6a). The background vorticity field also begins to converge towards the left portion of the domain. Figure 6b shows the two strip ends break apart and become more organized. Weak vorticity values replace the original high vorticity values in the center of the domain. Background vorticity begins to increase in certain areas with a segment of notable vorticity forming on the right side of the domain and to the southeast of the right vorticity max. This feature is occasionally close enough to modify the development of the right vorticity max (Fig. 6c). The left-most vortex begins to propagate towards the west-southwest, developing an area of weak vorticity on the northeastern side and stronger vorticity on the southwestern edge of the vortex (Figs. 6c and 6d). The area of weak vorticity from Figure 6b wraps around the right vorticity max and develops on the northeastern end of the vortex, removing the notable vorticity area that appeared on the right side of the vortex earlier in the simulation (Figs. 6c and 6d). This behavior mimics what was seen earlier around the left vortex, however the right vortex generates a more defined area of vorticity on the southwest edge of the vortex maximum. (Fig. 6d). By the end of the model run, the area develops into a tail of higher vorticity air behind the right vortex on the southwestern side complementing the weak vorticity on the northeast side (Fig. 5e).

4. DISCUSSION AND CONCLUSIONS

These experiments shed some light on the evolution of finite vorticity strips. In the *f*-plane simulations, no fixed length-to-width ratio was found that clearly determined when a strip breaks down into two vortices rather than roll up into one. This was true in the 6.25×10^{-5} s^{-1} constant vorticity cases and the 12.5 m/s maximum wind case. The initial widths of the vorticity strips, however, appear to play a role in determining at what length-to-width ratio the vorticity strips break down into two vortices. The findings of this study indicated wider strips separate into two vortices at lower length-to-width ratios than thinner strips. The width also has a positive effect on the strength of the resulting vortices whereas the length of the strip affects the vortex size and the corresponding cyclonic wind field coverage. The area of positive vorticity is noticeably larger in areal extent at the end of the *f*-plane experiments with longer strips, whether the initial strips breaks into two or rolls up into one vortex.

The *β*-plane experiments diverge rapidly from the *f*-plane simulations. The maximum vorticity value specified (in this case 6.25×10^{-5} s^{-1}) drastically affects the results of the β simulations. The Coriolis effect at 10°N significantly influences such weak values of

vorticity. Stronger vorticity values are less affected by β (not shown). In this case, β immediately began to act as the left side of the vorticity strip rotated southward, pooling high vorticity values towards the west. This is expected as the wind advects higher vorticity air from the north to the south. The opposite occurs on the right side of the vorticity maximum, as the wind advects lower vorticity air up from the south. This causes the formation of the weak area of vorticity depicted in Figure 5b as the two vortices separate. Examining the left vortex, an area of minimal vorticity forms on the northeast side of the vorticity maximum along with an area of higher than background vorticity on the southwest side (Fig. 5d). Judging by the general north-northwest movement of the vortex near the end of the simulation, this phenomenon appears similar to the β-gyres described in Willoughby et al. (1992). Similar structures and movement patterns are seen on the right vortex as well (Figs. 5d and 5e).

Both left and right vortices form elongated areas of higher vorticity on the southwest side of each maximum (Figs. 5d and 5e). These areas are similar to the tails observed by Wang et al. (2010) but without moist dynamics. Areas of higher vorticity also form away from the main vortices. The first disassociated area forms in Figure 5b to the southeast of the right vortex as well as in the northwest portion of the domain. A second area appears at the right edge of the domain and persists throughout the simulation. Both areas appeared regardless of the dimensions of the initial vorticity strip. Similar localized vorticity maxima spawn in various locations across the domain during the *β*-plane model runs (Figs. 5c, 5d, and 5e). In some cases, these localized vorticity maxima appear to affect the evolution of the initial vorticity strip.

This study looks to analyze the evolution of finite vorticity strips in light of the significant research surrounding the breakdown of the ITCZ. This research suggests that elliptical strips of constant vorticity do not break down at a given ratio of length and width for all strip sizes on an *f*-plane. Higher ratios are needed for thinner strips to undergo vortex separation than wider strips. Constant maximum wind cases mirror those results but evolve at different rates. Finite vorticity strip evolution within a *β*-plane is starkly different from an *f*-plane. The Coriolis force acts to create β-gyres around the vortices and generates areas of higher vorticity within the background. These curious sections of vorticity present an area of further study.

5. REFERENCES

Ferreira, Rosana Nieto, Wayne H. Schubert, 1997: Barotropic Aspects of ITCZ Breakdown. *J. Atmos. Sci.*, 54, 261–285.

Guinn, T.A., and W.H. Schubert, 1993: Hurricane spiral bands. *J. Atmos. Sci.*, 50, 3380-3403.

Schubert, Wayne H., Michael T. Montgomery, Richard K. Taft, Thomas A. Guinn, Scott R. Fulton, James P. Kossin, James P. Edwards, 1999: Polygonal Eyewalls, Asymmetric Eye Contraction, and Potential Vorticity Mixing in Hurricanes. *J. Atmos. Sci.*, 56, 1197–1223.

Wang, Chia-Chi, Chia Chou, Wei-Liang Lee, 2010: Breakdown and Reformation of the Intertropical Convergence Zone in a Moist Atmosphere. *J. Atmos. Sci.*, 67, 1247–1260.

——, and G. Magnusdottir, 2005: ITCZ breakdown in three-dimensional flows. J. Atmos. Sci., 62, 1497–1512.

Willoughby, H. E., 1992: Linear Motion of a Shallow-Water Barotropic Vortex as an Initial-Value Problem. J. Atmos. Sci., 49, 2015–2031.

6. FIGURES

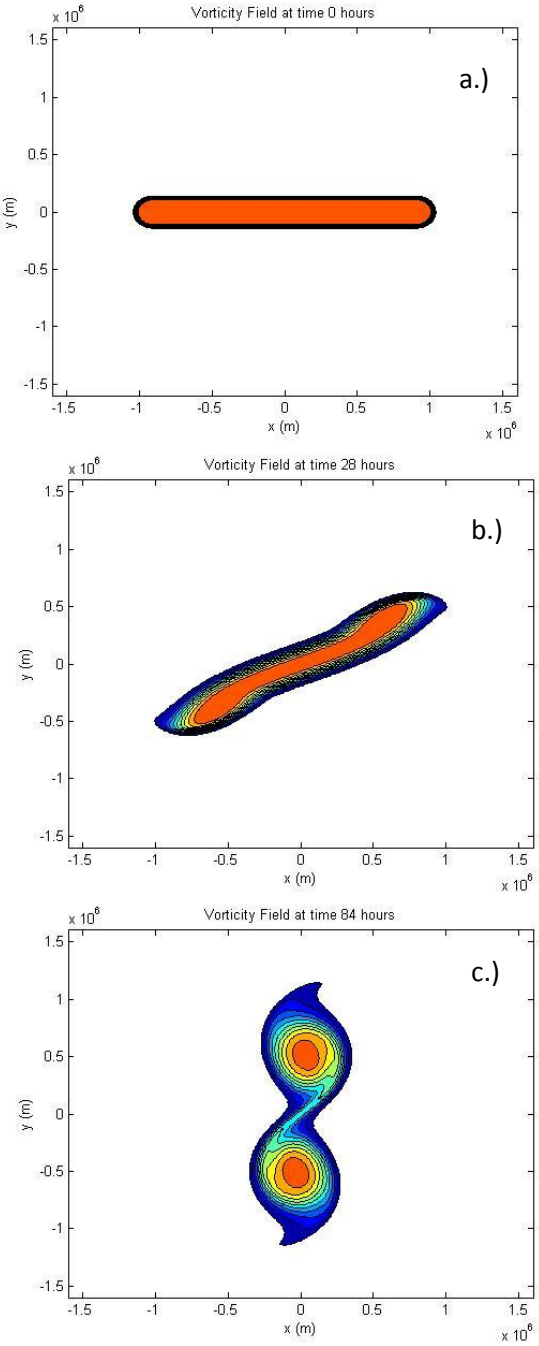

Figure 1. Vorticity evolution of a strip 1800 km long and 200 km thick. (a) The initial "Twinkie" finite strip. b) The vorticity field at (b) 28 hours and (c) 84 hours into the simulation.

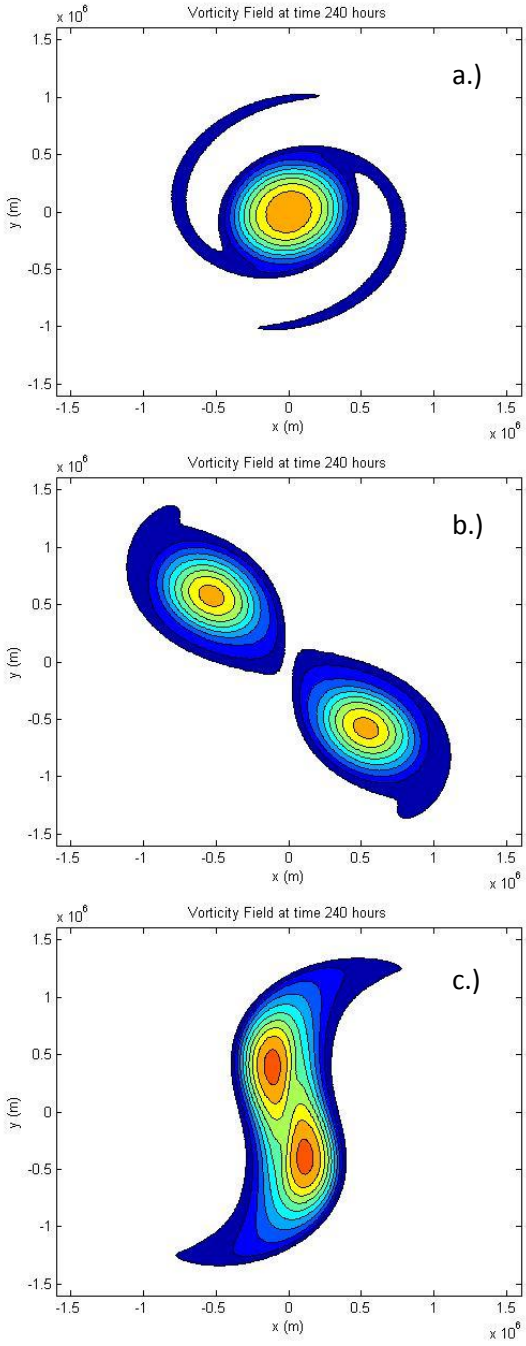

Figure 2. The vorticity field after 10 days for a) single vortex case, b) vortex separation case, and c) a merging case

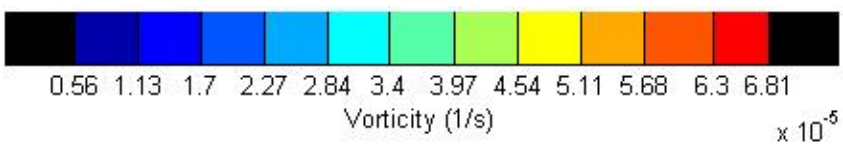

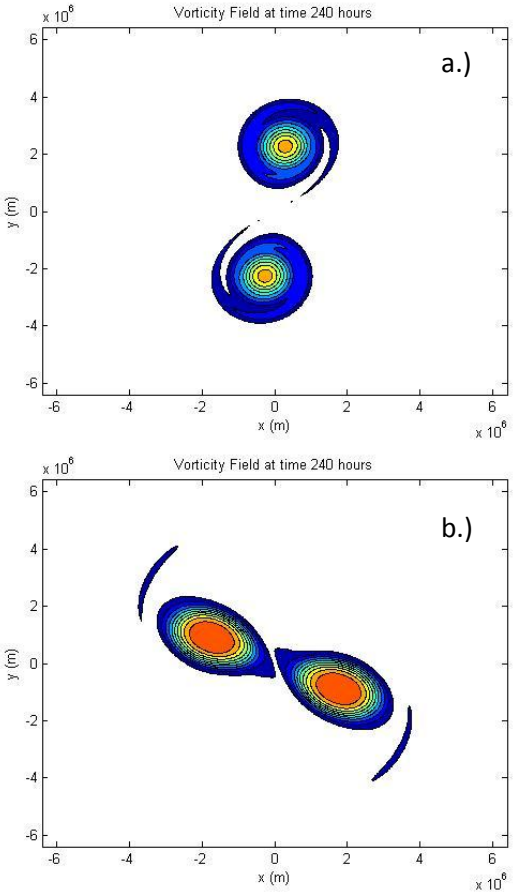

Figure 3. The vorticity fields at the end of 10 days for a.) a strip 4000 km long and 200 km thick and b.) a strip 3600 km long and 400 km thick.

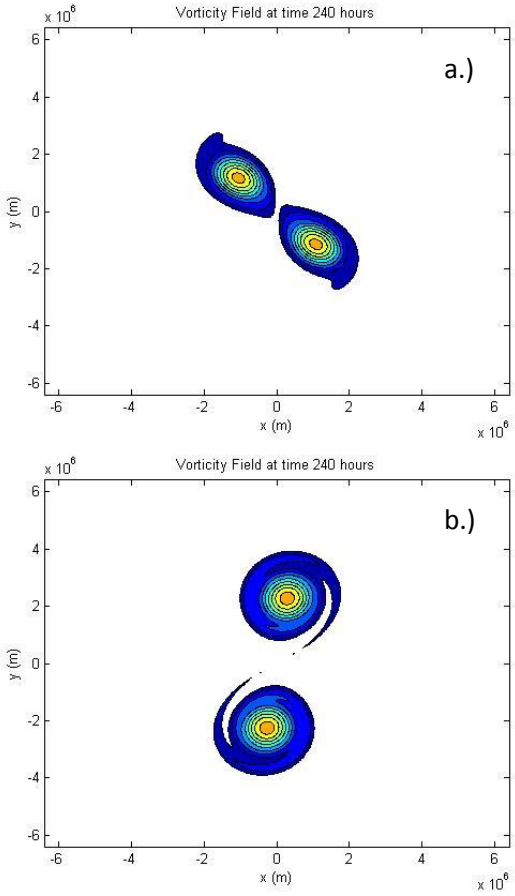

Figure 4. The vorticity field after 10 days for a.) a strip 2800 km long and 200 km thick and b.) a strip 4000 km long and 200 km thick

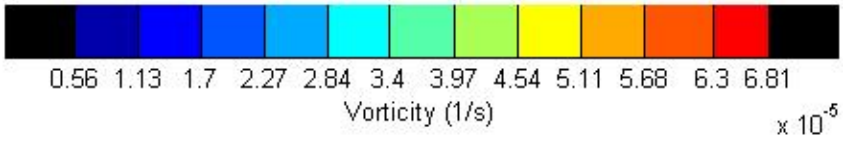

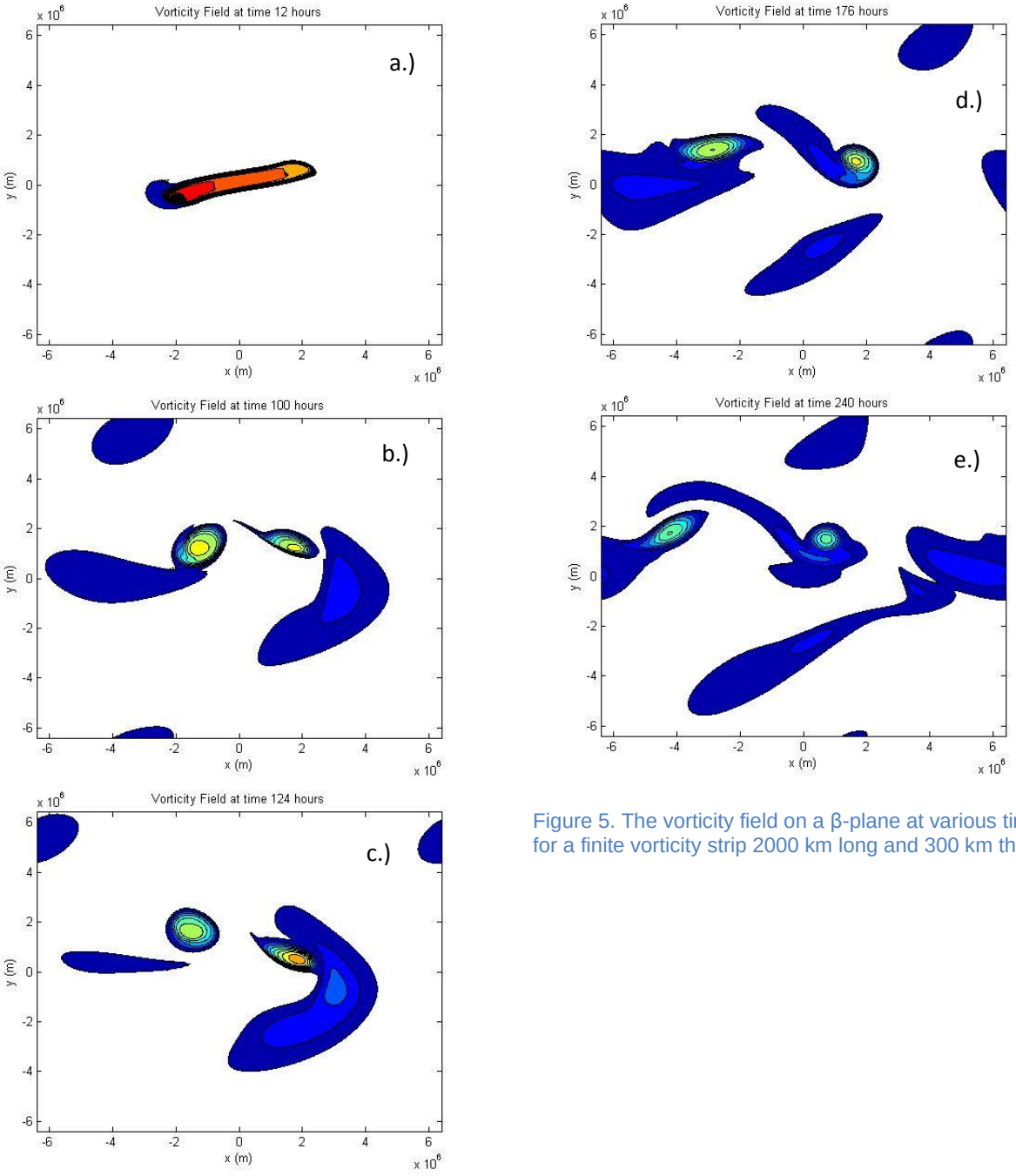

Figure 5. The vorticity field on a β-plane at various times for a finite vorticity strip 2000 km long and 300 km thick.